https://doi.org/10.5194/egusphere-2025-6247
Preprint. Discussion started: 22 December 2025

Analysis of factors influencing rockfall activity with a new method to estimate the release frequency in case of scarce data

Didier Hantz[1], Michel Jaboyedoff[2], Christine Moos[3], Luuk Dorren[3], Antoine Guerin[1,4], Antoine Guillemot[1,5], Jean-Pierre Rossetti[1,6], Marc Janeras[7]

[1]Univ. Grenoble Alpes, Univ. Savoie Mont Blanc, CNRS, IRD, Univ. Gustave Eiffel, ISTerre, 38000 Grenoble, France
[2]Risk-group, Institute of Earth Sciences, University of Lausanne, 1015 Lausanne, Switzerland
[3]Bern University of Applied Sciences, School of Agricultural, Forest and Food Sciences (BFH-HAFL), 3052 Zollikofen, Switzerland
[4] Norbert SA, Engineering Geology and Hydrogeology, 1920 Martigny, Switzerland
[5] Géolithe, Recherche Développement et Innovation, 38920 Crolles, France
[6] Alp'Géorisques, 38420 Domène, France
[7] Institut Cartogràfic i Geològic de Catalunya (ICGC), 08038 Barcelona, Spain

Correspondence to: Didier Hantz (dhantz38@gmail.com)

Abstract. Understanding the relationship between rockfall release frequency and volume is essential for quantitative hazard and risk analyses. The volume–frequency relationship is usually modelled with a power law distribution determined by an exponent and an activity parameter that can be estimated based on volume distributions from rockfall event inventories. Here, a new method is presented, which allows for the estimation of a confidence interval for the activity parameter, even if the inventory contains a small number of events. It was applied to estimate the spatio-temporal frequency of failures larger than 1 m^3 for 22 natural mountain rock walls located in temperate climate zones and below the permafrost area. The obtained frequencies were similar to those given by power law fitting of the inventories. The meta-analysis showed that these frequencies vary by at least three orders of magnitude from 0.01 to 20 $yr^{-1}.hm^{-2}$, depending mainly on the geomorphological context of the cliff, the homogeneity of the cliff and the joint spacing. The exponent of the power law varies between 0.3 and 1.0 and tends to be lower for massive rock than for bedded rock. A primary classification is proposed that enables an estimation of the volume–frequency relationship parameters when no inventory is available. More inventories are needed to enhance this classification.

https://doi.org/10.5194/egusphere-2025-6247
Preprint. Discussion started: 22 December 2025

Graphical abstract

- **New method to estimate a confidence interval for the release frequency of rockfalls, even with a few events**

Example: Spatio-temporal frequency of failures larger than 1 m³ (A_{st}) for 18 rock walls (number of failure per year per hm²)

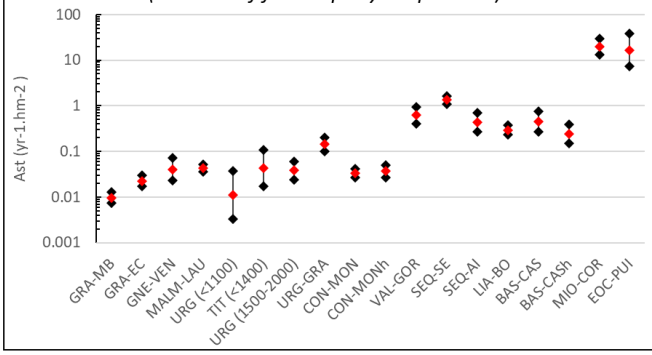

- **Meta-analysis of 22 natural mountain rock walls located in temperate climate zone and below the permafrost**
- **The release frequency depends mainly on the geomorphological context of the cliff, the joint spacing and the homogeneity of the cliff**

Classification to estimate the release frequency without rockfall inventory (homogenous cliffs)

Group	Joint spacing (m)	Maximal possible block volume (m³)	Ast (cliff above a stable slope)	Ast (cliff above an active landslide or gully)
1	>2	Hundreds of m³	0.01-0.1	0.1-1
2	0.6-2	Tens of m³	0.05-0.5	0.5-5
3	0.2-0.6	Some m³	0.2-2	2-20

1 Introduction

Failures in rock walls occur due to different mechanisms, such as sliding, toppling, bending or buckling (Hoek and Bray, 2001; Wyllie, 2017). Failure causes are described, for example, by Popescu (1994) and Loew et al. (2022). Depending on the underlying slope and the volume of the unstable rock compartment, failure can evolve into the fall of single rock fragments, rock mass falls or rockslides. These movements can be extremely rapid (Bourrier et al., 2013; Hungr et al., 2014) and create risks for buildings or people.

A quantitative assessment of the failure frequency for diffuse rockfall hazard (i.e., rockfalls from a rock wall without a specific source location) or the failure probability for localized rockfall hazards (i.e., rockfalls with a specific source location) is essential for realistic hazard and risk analyses (Hungr et al., 1999; Fell et al., 2008; Corominas et al., 2014; De Biagi et al., 2017a; Scavia et al., 2020; Jaboyedoff et al., 2021; Hantz et al., 2021). As rockfalls are the most noticeable slope movements occurring on rock walls, the failure frequency is usually analysed through rockfall event inventories. These can include records of rockfalls observed in the field or reconstructed based on historical data sources (e.g., Dussauge-Peissier et al., 2002; Melzner et al., 2023) as well as based on the monitoring of rock walls with, e.g. laser scanning or photogrammetry (e.g., Guerin et al., 2020; Janeras et al., 2023). Methods based on the measurement of deposited blocks do not allow for the determination of the failure frequency, because a failure usually releases rock masses consisting of several individual blocks that propagate downslope after fragmentation (Moos et al., 2022). Methods for the analysis of failure inventories are described, for example, by Graber and Santi (2022) or Janeras et al. (2023).

https://doi.org/10.5194/egusphere-2025-6247
Preprint. Discussion started: 22 December 2025

In general, a decreasing frequency with increasing rock volume can be observed. Many authors used a power law to model the volume–frequency relationship (e.g., Hungr et al., 1999; Dussauge-Peisser et al., 2002). Most of them focused on the value of the exponent of the power law, which reflects the uniformity of the volume distribution, rather than the level of rockfall activity (failure frequency), which is essential for hazard and risk analyses (cf. Graber and Santi, 2022).

Using published analyses of rockfall inventories obtained from terrestrial laser scanning (TLS), photogrammetry or historical reports, this paper presents values of the two parameters of the volume–frequency relationship (failure frequency and exponent) obtained for 22 different natural sites located in temperate climate zones and below the current permafrost limit (all are below 2500 m a.s.l.), and links these values to geological and geomorphological contexts. Thus, the objective of this study is to provide a method for the estimation of the failure frequency within a confidence interval for rock walls, even where the inventory contains a small number of events.

The main results of this work were presented by Hantz et al. (2024) at the 14th International Symposium on Landslides in July 2024. Phillips and Walton (2025) presented a meta-analysis of 44 rockfall inventories from the literature to explore the individual factors that affect the failure frequency, including natural slopes and cut slopes.

2 Method

2.1 Definition of a failure event

The volume of a failure can be determined by comparing the pre-failure and post-failure surfaces in the cliff or by estimating the total volume of the deposited material. A failure event is therefore defined as the detachment of a rock volume from a cliff between two dates, from a unique scar. Van Veen et al. (2017) and Williams et al. (2019) pointed out that in cases of regressive failure, neighbouring events occurred within a single monitoring interval are recorded as one. Thus, the number and the volumes of the rockfalls occurred in a cliff may depend on the monitoring interval, which must be considered when deriving rockfall volume–frequency relationships. Regressive failure events may last for several months or years (Janeras et al., 2017; Guerin et al., 2020). The observations of Van Veen et al. (2017) and Williams et al. (2019) were made for a hazardous slope consisting of highly weathered and foliated gneiss with tonalite dykes and dioritic intrusions, and for an actively eroding coastal cliff made of interbedded shale, sandstone and mudstone, respectively. D'Amato et al. (2016) detected 845 scars from an annual TLS survey in a limestone cliff located in a temperate climate zone, below the permafrost limit and above a stable talus slope (site SEQ-SE of this study). Continuous photographic monitoring allowed for the dating of 214 scars, with a temporal resolution between 10 min and 25 days to check if these scars resulted from distinct failure events. They all appeared as single events, which indicates that combined failures are rare in this type of limestone cliff.

A failure event typically results in several rockfall events at different locations in the underlying slope, which can be defined as the passage (or the landing) of one or several rock fragments. Its characteristics (frequency, volume, velocity, height, …) depend on the considered location in the slope and its width. The volumes of these rockfall events are usually smaller than the initial failure volume.

https://doi.org/10.5194/egusphere-2025-6247
Preprint. Discussion started: 22 December 2025

Please use only the styles of this template (MS title, Authors, Affiliations, Correspondence, Normal for your text, and Headings 1–3). The title page must include the title (concise but informative), author first and last names, full institutional addresses of all authors, and correspondence email for proofs. Deceased co-authors should be marked accordingly. After the abstract, the sequence of the sections of your manuscript is introduction, sections of your choice, and conclusions.

2.2 Failure activity

The simplest way to characterise rock-wall activity is to count failures over a sufficiently long observation period so that a meaningful number of events is recorded. Activity can be expressed as the number of failures with a minimum volume which occur per year for a rock wall of a given extent (temporal frequency). The minimum volume is the smallest measurable or appropriate volumethat potentially produces sufficient damage at the given study site. When a diffuse hazard is considered (failures occurring everywhere in the studied rock wall), a spatio-temporal frequency – the number of failures per unit of time and area – can be defined for a homogeneous zone. This spatio-temporal frequency can be used to characterise rock walls with similar features. It is estimated using a sampling area and period, which should be long enough to smooth temporal and spatial activity variations. For rock walls with low rockfall activity, the time window or the investigated wall area often needs to be extended to capture enough events. In some cases, the observations of separate similar rock walls can be combined to obtain a sufficient number of events. Janeras et al. (2023) introduced the concept of sampling extent, which is the sampling duration multiplied by the sampling area.

2.3 Direct estimation of the mean failure frequency

As the number of failures occurring in one year (or in a given time) is not constant, the temporal failure frequency F_t can be defined as the mean number of failures per unit of time. The number of failures expected in a period of length T is a random variable with a mean of $F_t \cdot T$. Following Durville (2004), Rat (2006) and De Biagi (2017), one can assume in a first approach that in a homogenous area, where a lot of independent rock compartments are at different evolutionary stages, the occurrence of failures is stationary at a yearly scale and is described by a Poisson law. Note that at a daily scale, the dates of the rockfall events are not independent because several rockfalls can be triggered by the same meteorological episode. If μ (= $F_t \cdot T$) is the mean number of failures that occur in a given duration, the probability that N failures occur is:

$$Poisson(P(\mu|N)) = \exp(-\mu)\mu^N/N! \quad (1)$$

However, the number of failures detected in an observation period of length T is usually not equal to μ, since the observation period is often too short for a precise estimation of μ. The observed number of failures N_{obs} provides information about μ and can be used in Bayes' theorem for continuous random variables. Using this theorem, the probability distribution of μ (continuous variable) can be determined from the observation of N failures (posterior probability):

$$P(\mu|N) = \frac{Poisson(N/\mu)P(\mu)}{\int Poisson(N/\mu)P(\mu)d\mu} \quad (2)$$

https://doi.org/10.5194/egusphere-2025-6247
Preprint. Discussion started: 22 December 2025

P(μ) is the "prior probability", which describes the probability of μ before the inventory is known. Here, we assumed that P(μ) is uniform in the interval of possible values of μ ("flat prior"). As P(μ) is a constant, the posterior probability becomes:

$$P(\mu|N) = \frac{\exp(-\mu)\mu^N}{N!} = PDF_{Erlang}(\mu, N+1,1) \quad (3)$$

The term PDF_{Erlang} denotes the probability density function of the Erlang distribution, which is a special case of the gamma distribution where the distribution shape is discretised. Here the rate parameter is equal to 1. The mode, mean and variance of μ are N, N+1, and N+1, respectively.

A 95% confidence interval for μ can be determined from the cumulative distribution function (CDF):

$$CDF\big(P(\mu|N)\big) = \frac{\int_0^{\mu} \exp(-t)t^N dt}{N!} = CDF_{erlang}(\mu, N+1,1) \quad (4)$$

Figure 1 shows the cumulative distribution function of μ for three values of N, and the 95% confidence interval for N = 10. It can be seen that the higher the N, the smaller the confidence interval of log(μ).

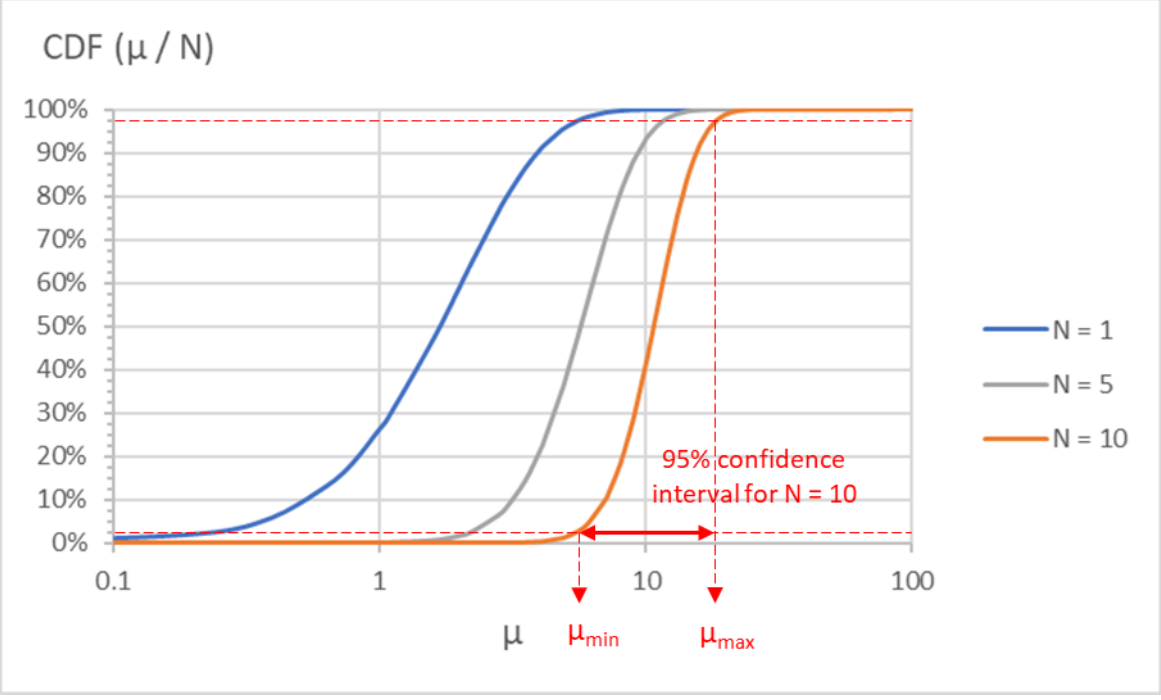

Figure 1: Cumulative distribution function of the Poisson parameter μ, given the observed number of failures N, where 95% confidence interval is highlighted for N = 10.

Table 1 gives the minimum and maximum estimations of the mean number of events μ for N_{obs} = 0 to N_{obs} = 10. Since the frequency is usually represented by its logarithm, the geometric mean and uncertainty factor are given. The Joint ISSMGE, ISRM and IAEG Technical Committee on Landslides and Engineered Slopes recommends qualifying the hazard level according to the decimal logarithm of the rockfall frequency (Fell et al., 2008, Table 5). From one hazard level to the next, the rockfall frequency is multiplied by 10. An uncertainty factor of 10 therefore corresponds to an uncertainty of one hazard level.

https://doi.org/10.5194/egusphere-2025-6247
Preprint. Discussion started: 22 December 2025

Even an inventory with only one recorded rockfall (N_{obs} = 1) has a far smaller uncertainty factor. This shows that even a small, exhaustive inventory can inform the hazard level.

To satisfy Poisson's hypotheses, the mean number of failures occurring during any period of the same duration as the observation period is assumed to be constant (constant mean frequency), and failures are assumed to be independent. Although mean annual frequency may vary because triggering conditions differ from year to year, rockfalls are surficial instabilities produced by long-term degradation of the rock mass. Therefore, the intensity of triggering factors is only partially related to the number and magnitude of failures. Thus, as a first approximation, the mean frequency can be estimated from a one-year observation period, provided that the observation area is large enough. Alternatively, or even complementarily, extending the observation period increases confidence in satisfying the hypotheses.

Note that if a regressive failure occurs in a one-year observation period, the constituent individual failures are not independent. If these individual failures account for a significant part of the observed failures, the period cannot be used to estimate the mean annual frequency. In the case of a very large progressive failure that lasts several months or years, the mean frequency in the scar may be of interest.

As frequency generally decreases with increasing volume, the uncertainty of the inverse cumulative frequency increases with volume, as illustrated in Figure 2 for a hypothetical inventory that follows a power law (note that in real inventories, the points are never perfectly aligned). This explains that the points corresponding to the largest observed volumes often deviate (above or below) from the fitted power law. Another reason for these points to be below the fitted power law may be that they are close to the maximal volume that can occur in the considered cliff (which depends mainly on its height). The explanation is thus: Suppose the observation period for the inventory of Figure 2 is multiplied by 10. Theoretically, one can expect the values of μ are multiplied by 10 and one event with volume larger or equal to 100,000 m^3 appears represented by a new point aligned with the rest. But if the maximal possible volume is 20,000 m^3, the new point will be under the alignment of the other points.

Table 1: Minimum (μ_{min}) and maximum (μ_{max}) estimations of the mean number of failures for a given duration, as a function of the observed number (N_{obs}) (using Poisson's law), geometric mean (μ_{gm}) and uncertainty factor.

Observed number (N_{obs})	0	1	2	3	4	5	6	7	8	9	10
μ_{min}	0	0.24	0.62	1.1	1.6	2.2	2.8	3.5	4.1	4.8	5.5
μ_{max}	3	5.6	7.2	8.8	10.2	11.7	13.1	14.4	15.8	17.1	18.4
Geometric mean (μ_{gm})		1.16	2.11	3.11	4.04	5.05	6.06	7.10	8.05	9.06	10.1
Uncertainty factor (μ_{max}/ μ_{gm})		4.83	3.41	2.83	2.52	2.31	2.16	2.03	1.96	1.89	1.83

https://doi.org/10.5194/egusphere-2025-6247
Preprint. Discussion started: 22 December 2025

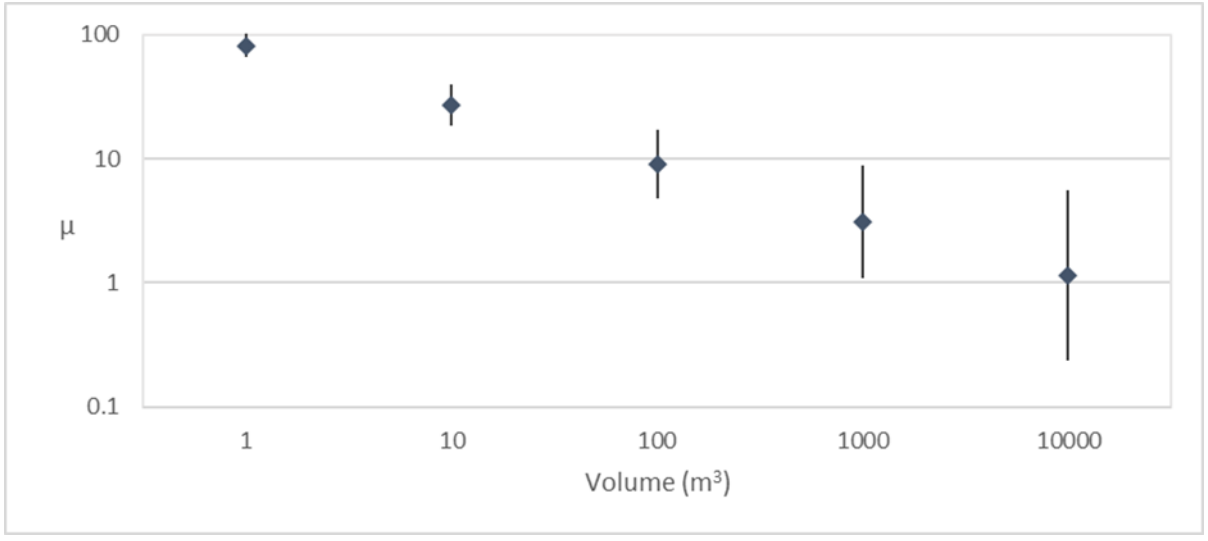

Figure 2: Estimation of the mean number of failures (μ) (and confidence interval) as a function of failure volume for a hypothetical inventory comprising 81, 27, 9, 3, and 1 observed failures for respective minimum volumes of 1, 10, 100, 1000 and 10,000 m³.

2.4 Volume distribution

A comprehensive description of failure activity for hazard assessments requires evaluating the frequencies across different volume intervals. As the frequency decreases with increasing volume, the sampling extent must sometimes be increased. The volume distribution can be described by a histogram, showing the observed number of failures for different volume intervals, or by a cumulative distribution function (or a density function). In this work, we use the inverse cumulative distribution function that gives the number of failures N with a volume larger or equal to V. Many authors proposed to model the empirical distribution with a power law distribution. Its inverse cumulative distribution can be expressed as

$$N = A_0 (V/V_0)^{-B} \quad (5)$$

where N is the number of failures with a volume larger or equal to V, B reflects the uniformity of the distribution and A_0 is the number of failures with a volume larger or equal to a reference volume V_0. A_0 represents the overall failure frequency and, thus, the rock wall activity. In this study, we consider a reference volume of 1 m^3 because most failure inventories include events of this order of magnitude and these events are relevant for risk analyses (Scavia et al., 2020; Dorren et al., 2022). For example, the French guidelines for rockfall hazard assessment in land-use planning considers that important damages to buildings occur for block volumes larger than 1 m^3 and that volumes smaller than 0.05 m^3 cause very few damages (MEZAP, 2021). When V_0 = 1 m^3, N can be written as

$$N = A\, V^{-B} \quad (6)$$

where A is the number of failures with a volume larger or equal to 1 m^3. The temporal failure frequency F_t is obtained by dividing N by the length of the observation period, T_{obs}:

$$F_t = N / T_{obs} = A_t\, V^{-B} \quad (7)$$

https://doi.org/10.5194/egusphere-2025-6247
Preprint. Discussion started: 22 December 2025

Note that the observation period should be independent of the observations, which is generally satisfied for instrumental monitoring. But in historical inventories the observation period is often considered from the first to last event. Then, the mean frequency should be computed as $(N-1)/T_{obs}$, or, alternatively, T_{obs} should be defined differently (Janeras et al., 2023).

To compare different rock walls, it is useful to consider the spatio-temporal frequency F_{st} (Hantz et al., 2003), which is the number of failures per unit of time and per unit of (inclined) wall surface (S_w) or wall width, written as

$$F_{st} = N / T_{obs} / S_w = A_{st} V^{-B} \quad (8)$$

In this study, we express F_{st} as the number of events per year and per hm^2 ($1\ hm^2 = 10^4\ m^2$), which allows to concretise the activity of a given area of rock wall being assessed. Note that the concept of spatio-temporal frequency should be applied to rock walls that are relatively homogenous.

Ideally, the observation period should be long enough to include the maximum possible failure volumes of a rock wall. When the length of this period increases, larger failures may occur up to a maximal possible volume, which mainly depends on the height of the rock wall. Ideally, the observation period should be longer than the return period corresponding to this maximal possible volume. If it is much longer, the volume of the largest failures observed will not increase according to the power law, but the number of failures close to the maximum possible volume will increase. Therefore, the power law (Eq. 6) must be truncated at the maximum possible volume V_{MAX}:

For $V <$ or $=$ to V_{MAX}, $N = A\ V^{-B}$;

For $V > V_{MAX}$, $N = 0$.

2.5 Estimation of the failure frequency using the power law model

Assuming that the rockfall volume distribution follows a power law for a certain volume range, the consideration of the whole observed volume range (including volumes smaller than the volume of interest) will improve the estimation of the failure frequency, because more information is considered. Moreover, the extrapolation of the power law allows to estimate the frequency of volumes that are outside the observed volume range. Extrapolation can be used, for example, when the volume of interest is too small to be detected with the inventory method used or to estimate the frequency of larger volumes than observed when the observation period is short.

3 Data

3.1 Data acquisition

The data used in this study originates from studies that analysed the frequency of failures or rockfall events in continental natural rock walls located below the permafrost limit and at latitudes from 40 to 50° North. We have excluded failures in rock cuts and inventories of deposited individual blocks, as the focus of this study is to characterise the failure frequency of rock masses releasing from rock walls, rather than the frequency of their fragments. We have selected studies that explicitly provided the activity parameter A or alternatively sufficient data that allowed for its estimation. Most inventories are derived

https://doi.org/10.5194/egusphere-2025-6247
Preprint. Discussion started: 22 December 2025

from instrumental monitoring (terrestrial laser scanner or photogrammetry), but some are historical inventories with an approximate estimation of the volume.

For each study site, we calculated the mean A_{st} (yearly frequency per area) and its confidence interval. If the confidence intervals of the frequencies observed in different cliffs belonging to the same massif were compatible, we considered these cliffs as a unique cliff (French Tithonian cliffs, French Urgonian cliffs, Montserrat). This allowed for a higher number of failures and consequently a smaller confidence interval.

3.2 Studied cliffs

The different sites considered in this study are briefly presented hereafter and some characteristics are given in Tables 2 and 3. When different cliffs were considered as a unique cliff, the durations of the observation periods are usually different and no duration is given in Table 2. We have used the spacing intervals suggested by ISRM (1981). The joint spacing refers to bed (or layer) thickness for layered rock masses or to fracture intercept (mean distance between successive joints as measured along a straight line) in other cases. The joint spacing given in Table 3 was estimated from quantitative or qualitative descriptions given in the different sources.

https://doi.org/10.5194/egusphere-2025-6247
Preprint. Discussion started: 22 December 2025

Table 2: Characteristics of the study sites. Acronyms refer to the lithology or the stratigraphy and the location of the cliff. The letter h at the end refers to historical inventories.

Location	Country	Acronym	Reference	Lithology	Cliff area (hm^2)	Duration (yr)	Sampling extent ($hm^2.yr$)
Middle Brother	USA	GRA-MB	Guerin et al., 2020	granitic rock	90	40	3600
El Capitan	USA	GRA-EC	Guerin et al., 2020	granitic rock	47	41	1927
Venosc	F	GNE-VEN	Hantz & Levy, 2019	gneiss	38	7	266
Lauterbrunnen	CH	MALM-LAU	Mohadjer et al. 2020	limestone	520	5.2	2704
French Urgonian cliffs (<1100 m)	F	URG (<1100)	Epinat, 2016; Guillemot, 2017; this study	limestone	51.2		190
French Tithonian cliffs (<1400 m)	F	TIT (<1400)	Hantz & Levy, 2019; this study	limestone	22.85		96
French Urgonian cliffs (1500-2000 m)	F	URG (1500-2000)	Alber, 2016; this study	limestone	39		468
Mont Granier North face	F	URG-GRA	Alber, 2016; Hantz & Levy, 2019	limestone	15	16	240
Montserrat	E	CON-MON	Janeras et al., 2023	conglomerate	9.05		72
Montserrat (historical)	E	CON-MONh	Janeras et al., 2023	conglomerate	86.8		1080
Gorgette gully	F	VAL-GOR	Hantz & Levy, 2019	limestone	5.1	6.9	35
Mont Saint-Eynard South	F	SEQ-SE	Hantz & Levy, 2019; this study	limestone	12.3	5.7	70
Mont Saint-Eynard Aiguille	F	SEQ-AI	Hantz & Levy, 2019	limestone	9.9	3.7	37
Bourg d'Oisans, Bassey	F	LIA-BO	Hantz & Levy, 2019	limestone	82.7	3.1	256
Castellfollit	E	BAS-CAS	Janeras et al., 2023	columnar basalt	2.4	13	31
Castellfollit (historical)	E	BAS-CASh	Janeras et al., 2023	columnar basalt	4.14	16	66
La Cornalle	CH	MIO-COR	Carrea et al., 2021	sandstone-marl	0.22	5	1.1
Puigcercós	E	EOC-PUI	Abellan et al., 2010; Blanch, 2015	marl-sandstone-clay	0.375	0.8	0.3
Exhaustive from a volume much larger than 1 m^3							
Andorra	AND	GRA-AND	Corominas et al., 2018; Santana et al., 2012	granodiorie, hornfels	4.2	19	80
Illgraben	CH	QUA-ILL	Bennett et al., 2012	quartzite	70	19	1330
French Tithonian cliffs (<1400 m)	F	TITh (<1400)	Hantz & Levy, 2019; this study	limestone	365	22	8030
French Urgonian cliffs (<2000 m)	F	URGh (<2000)	Alber, 2016; this study	limestone	2451	17	41667

220

https://doi.org/10.5194/egusphere-2025-6247
Preprint. Discussion started: 22 December 2025

3.2.1 Granitic and gneissic rocks

Guerin et al. (2020) obtained volume–frequency relationships for two cliffs made up of massive granitic rocks in the Yosemite Valley (USA) using terrestrial laser scanning and photogrammetry.

Hantz and Levy (2019) derived a volume–frequency relationship from TLS for a massive gneissic rock wall in the Massif des Ecrins (France).

Corominas et al. (2018) developed a volume–frequency relationship from a historical inventory of a rock wall in Andorra made up of highly fractured granodiorite and hornfels. Santana et al. (2012) analysed spacing of the discontinuities.

3.2.2 Mesozoic limestone and dolostone

The analysed data concern anaclinal cliffs, orthoclinal cliffs or slowly dipping cataclinal cliffs (no sliding on bedding planes). The bed thickness varies from very large (> 2 m) to moderate (0.2 to 0.6 m) according to ISRM (1981). The compressive strength of these rocks is high (> 60 MPa) according to ISRM (1981).

Hantz and Levy (2019) reported data from limestone cliffs of various geological stages in the French Alps (Liassic, Sequanian, Tithonian, Valanginian and Barremian). Most of these formations are commonly encountered in the Subalpine Chains of the European Alpine Arc (geological maps Domène, Grenoble, Annecy-Ugine, Vizille). Data came from terrestrial laser scanner surveys and photogrammetric surveys. Details on the methodology used to detect the failures and on the inventories are given in Guerin et al. (2013), D'Amato (2015), D'Amato et al. (2016) and Hantz et al. (2019, 2020b). Tithonian cliffs and Barremian cliffs (Urgonian facies) are mainly made up of massive limestones (bed thickness > 2 m), whereas Sequanian and Liassic cliffs are made up of beds of moderate thickness (0.2 to 0.6 m). The studied Valanginian cliff is made up of beds of large thickness (0.6 to 2 m) and is underlain by an active gully. Cliffs with similar lithology, structure and climate (altitude and latitude), and for which the confidence intervals of the failure frequency have a common intersection, were assumed to be similar enough to be grouped in a unique inventory (French Urgonian cliffs, French Tithonian cliffs).

Hantz and Levy (2019) presented historical inventories for the Tithonian and Urgonian cliffs of the Chartreuse and Vercors massifs in France.

Mohadjer et al. (2020) derived volume–frequency relationships using a terrestrial laser scanner of upper Jurassic (Malm) massive limestone cliffs in the Helvetic zone in Switzerland.

3.2.3 Eocene conglomerate

Janeras et al. (2023) presented rockfall inventories for different cliffs of the Montserrat Massif close to Barcelona (Spain), made up of an Eocene conglomerate and monitored with TLS. The more productive cliff (Degotalls North) was not considered here because a lot of rockfalls resulted from a larger event and then were not independent. Also, this cliff cannot be considered as homogenous, because rockfalls concentrated in or around the scar of the large event (Janeras et al., 2017). In the other cliffs, 367 failures smaller than 1 m^3 were detected.

https://doi.org/10.5194/egusphere-2025-6247
Preprint. Discussion started: 22 December 2025

A historical inventory was also available for the Montserrat massif. The area and time span covered by this inventory depend on the rockfall volume considered – both increase with rockfall volume (Janeras et al., 2023).

3.2.4 Columnar basalt

Abellan et al. (2011) and Janeras et al. (2023) studied a cliff made up of columnar basalt in Castellfollit de la Roca (Spain). Janeras et al. (2023) derived a volume–frequency relationship using terrestrial laser scanning for failure smaller than 10 m^3. Both used a historical inventory to estimate the frequency for larger volumes.

3.2.5 Heterogeneous Cenozoic cliffs

Carrea et al. (2021) derived a volume–frequency relationship using TLS for a cliff made up of alternating Miocene sandstone and marl beds, located near Lausanne (Switzerland). This cliff is the lateral scarp of an active landslide.

Abellan et al. (2010) monitored, using TLS, a cliff consisting of Eocene marl, sandstone, silt and clay, located in Puigcercós (Spain). It is the main scarp of a landslide which occurred in 1881 and is still active (Royan et al., 2015). They did not study the volume distribution but analysed the number of failures larger than 1 m^3; Blanch (2015) analysed the volume distribution.

3.2.6 Quartzite

Bennett et al. (2012) used digital photogrammetry to produce an inventory of rockslides and rockfalls that occurred at the head of the Illgraben, a very active catchment prone to debris flows in Switzerland.

4 Results

The obtained frequencies are presented in Table 3 and Figure 3 with 95% confidence intervals. The mean value of the frequency varies between 0.01 and 19.65 $yr^{-1}.hm^{-2}$, but the union of the 95% confidence intervals range from 0.007 to 38 $yr^{-1}.hm^{-2}$.

TLS monitoring of the Montserrat cliffs does not detect any rockfall larger than 1m^3. Without any additional information, the minimal possible frequency would be zero. But the historical inventory (CON-MONh) gives a minimal frequency of 0.027 $yr^{-1}.hm^{-2}$. This value was taken as the minimal value for the TLS inventory (CON-MON).

Some inventories are exhaustive from a volume much larger than 1 m^3, like for the sites of Andorra (GRA-AND) and Illgraben (QUA-ILL), and the French Tithonian and Urgonian cliffs (TITh and URGh). In such cases, the frequency of volume larger than 1 m^3 can only be extrapolated using the power law model. Overall, the modelled and the observed frequencies have the same order of magnitude (the ratio is between 0.66 and 1.48; Fig. 4 and Table 4). So, the frequencies obtained by extrapolation of the power law can be considered in the analysis.

Table 3: Spatio-temporal frequency of failures larger than 1 m^3 expressed in $yr^{-1}.hm^{-2}$ (last column). $A_{st\ min}$, $A_{st\ max}$: 95% confidence interval. Nb > 1m^3: Number of failures > 1 m^3.

https://doi.org/10.5194/egusphere-2025-6247
Preprint. Discussion started: 22 December 2025

Location	Acronym	Lithology	Stratigraphy, zone	Joint spacing (m)	Altitude (m)	Nb > 1m^3	$A_{st\,min}$	$A_{st\,max}$	$A_{st\,obs}$
Middle Brother	GRA-MB	granitic rock		>2	1300-2100	42	0.007	0.013	**0.010**
El Capitan	GRA-EC	granitic rock		>2	1500-2200	50	0.017	0.030	**0.023**
Venosc	GNE-VEN	gneiss		>2	1000-1800	11	0.023	0.072	**0.041**
Lauterbrunnen	MALM-LAU	limestone	Malm, Quinten, Helvetic	>2	800-1600	117	0.036	0.052	**0.043**
French Urgonian cliffs (<1100 m)	URG (<1100)	limestone	Barremian, Urgonian, Dauphinoise	>2	<1100	2	0.0033	0.038	**0.011**
French Tithonian cliffs (<1400 m)	TIT (<1400)	limestone	Malm, Tithonian, Dauphinoise	>2	<1400	4	0.0170	0.107	**0.043**
French Urgonian cliffs (1500-2000 m)	URG (1500-2000)	limestone	Barremian, Urgonian, Dauphinoise	>2	1500-2000	18	0.0244	0.061	**0.038**
Mont Granier North face	URG-GRA	limestone	Barremian, Urgonian, Dauphinoise	>2	1500-1900	35	0.102	0.203	**0.144**
Montserrat	CON-MON	conglomerate	Eocene	>2	700-900	0	0.027	0.042	**0.034**
Montserrat (historical)	CON-MONh	conglomerate	Eocene	>2	700-900	40	0.027	0.05	**0.037**
Gorgette gully	VAL-GOR	limestone	Valanginian, Dauphinoise	0.6-2	1350-1500	22	0.41	0.94	**0.62**
Mont Saint-Eynard South	SEQ-SE	limestone	Sequanian, Dauphinoise	0.2-0.6	850-1100	93	1.09	1.63	**1.33**
Mont Saint-Eynard Aiguille	SEQ-AI	limestone	Sequanian, Dauphinoise	0.2-0.6	850-1100	16	0.27	0.71	**0.44**
Bourg d'Oisans, Bassey	LIA-BO	limestone	Lias, Dauphinoise	0.2-0.6	900-1450	75	0.23	0.37	**0.29**
Castellfollit	BAS-CAS	columnar basalt		0.2-0.6	270-300	14	0.27	0.76	**0.45**
Castellfollit (historical)	BAS-CASh	columnar basalt		0.2-0.6	270-300	16	0.15	0.39	**0.24**
La Cornalle	MIO-COR	sandstone-marl	Miocene, Molasse	0.6-2	700-735	22	13	29.70	**19.65**
Puigcercós	EOC-PUI	marl-sandstone-clay	Eocene	0.2-0.6	500-530	5	7.2	38.00	**16.54**
Exhaustive only from a volume much larger than 1 m^3									
Andorra	GRA-AND	granodiorite, hornfels		0.2-2	1050-1300				
Illgraben	QUA-ILL	quartzite	Trias, Pennic	highly fractured	1250-2370				
French Tithonian cliffs (<1400 m)	TITh (<1400)	limestone	Malm, Tithonian, Dauphinoise	>2	<1400				
French Urgonian cliffs (<2000 m)	URGh (<2000)	limestone	Barremian, Urgonian, Dauphinoise	>2	<2000				

https://doi.org/10.5194/egusphere-2025-6247
Preprint. Discussion started: 22 December 2025

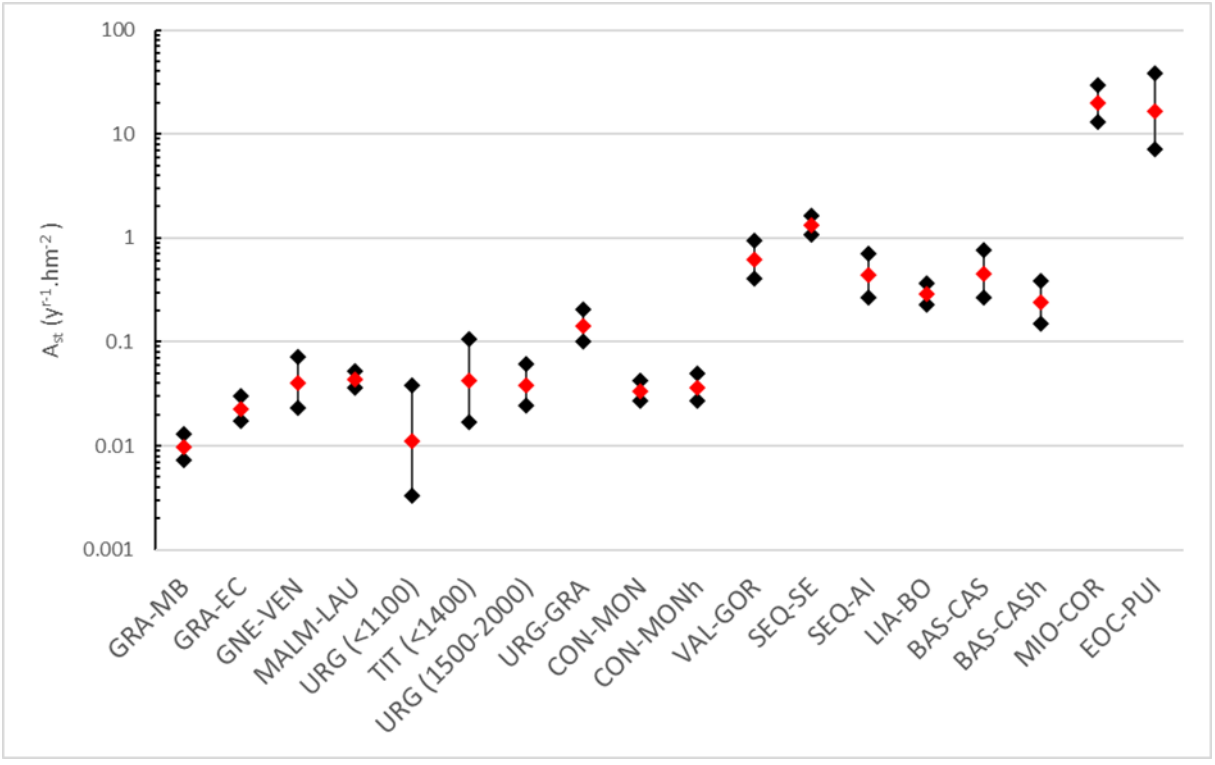

285 **Figure 3: Spatio-temporal frequency of failures larger than 1 m^3 expressed in $yr^{-1}.hm^{-2}$. The red points represent the geometrical mean of the minimal and maximal values obtained with a 95% confidence interval (black points).**

https://doi.org/10.5194/egusphere-2025-6247
Preprint. Discussion started: 22 December 2025

Table 4: Comparison between the failure frequency observed ($A_{st\ obs}$) and the frequency derived from the power law model ($A_{st\ mod}$), both expressed in $yr^{-1}.hm^{-2}$. $A_{st\ min}$, $A_{st\ max}$: 95% confidence interval. Nb > $1m^3$: Number of failures > 1 m^3. Nb PL, V_{min}, V_{max}: Number of failures, minimal and maximal volumes considered for power law fitting. B: exponent of the power law.

Location	Acronym	Nb > $1m^3$	$A_{st\ min}$	$A_{st\ max}$	$A_{st\ obs}$	Nb PL	V_{min}	V_{max}	$A_{st\ mod}$	B	A_{stmod}/ A_{stobs}
Middle Brother	GRA-MB	42	0.0073	0.013	**0.010**	81	0.06	2.0E+04	**0.011**	0.32	1.13
El Capitan	GRA-EC	50	0.0172	0.030	**0.023**	70	0.24	1.0E+04	**0.023**	0.39	1.01
Venosc	GNE-VEN	11	0.023	0.072	**0.041**	25	0.05	2.3E+02	**0.050**	0.46	1.23
Lauterbrunnen	MALM-LAU	72	0.036	0.052	**0.043**	117	0.6	2.7E+02	**0.040**	0.66	0.92
French Urgonian cliffs (<1100 m)	URG (<1100)	2	0.0033	0.038	**0.011**	22	0.009	1.3E+00	**0.015**	0.5	1.34
French Tithonian cliffs (<1400 m)	TIT (<1400)	4	0.0170	0.107	**0.043**	17	0.027	1.6E+00	**0.031**	0.51	0.73
French Urgonian cliffs (1500-2000 m)	URG (1500-2000)	18	0.0244	0.061	**0.038**	19	0.90	4.0E+03	**0.043**	0.38	1.12
Mont Granier North face	URG-GRA	35	0.102	0.203	**0.144**	35	1	7.9E+02	**0.151**	0.4	1.05
Montserrat	CON-MON	0	0.027	0.042	**0.034**	289	0.003	5.0E-01	**0.049**	0.81	1.46
Montserrat (historical)	CON-MONh	7	0.027	0.05	**0.037**	18	0.001	5.0E+00	**0.026**	0.6	0.71
Gorgette gully	VAL-GOR	22	0.41	0.94	**0.62**	116	0.1	1.2E+03	**0.640**	0.65	1.03
Mont Saint-Eynard South	SEQ-SE	93	1.09	1.63	**1.33**	800	0.05	1.5E+03	**1.500**	0.78	1.13
Mont Saint-Eynard Aiguille	SEQ-AI	16	0.27	0.71	**0.44**	18	0.5	5.2E+01	**0.460**	0.67	1.05
Bourg d'Oisans, Bassey	LIA-BO	75	0.23	0.37	**0.29**	103	0.5	2.7E+01	**0.300**	1.01	1.03
Castellfollit	BAS-CAS	13	0.27	0.76	**0.45**	194	0.001	6.0E+00	**0.373**	0.44	0.82
Castellfollit (historical)	BAS-CASh	16	0.15	0.39	**0.24**	16	1	2.0E+03	**0.240**	0.5	0.99
La Cornalle	MIO-COR	22	13	29.70	**19.65**	300	0.01	4.0E+00	**23.600**	0.56	1.20
Puigcercós	EOC-PUI	5	7.2	38.00	**16.54**	42	0.001	8.7E+01	**10.700**	0.69	0.65
Exhaustive only from a volume much larger than 1 m^3											
Andorra	GRA-AND					16	4	4.5E+02	**0.450**	0.54	
Illgraben	QUA-ILL					497	233	1.6E+06	**12.000**	0.65	
French Tithonian cliffs (<1400 m)	TITh (<1400)					14	100	7.0E+03	**0.022**	0.61	
French Urgonian cliffs (<2000 m)	URGh (<2000)					14	1000	1.2E+05	**0.026**	0.7	

290

https://doi.org/10.5194/egusphere-2025-6247
Preprint. Discussion started: 22 December 2025

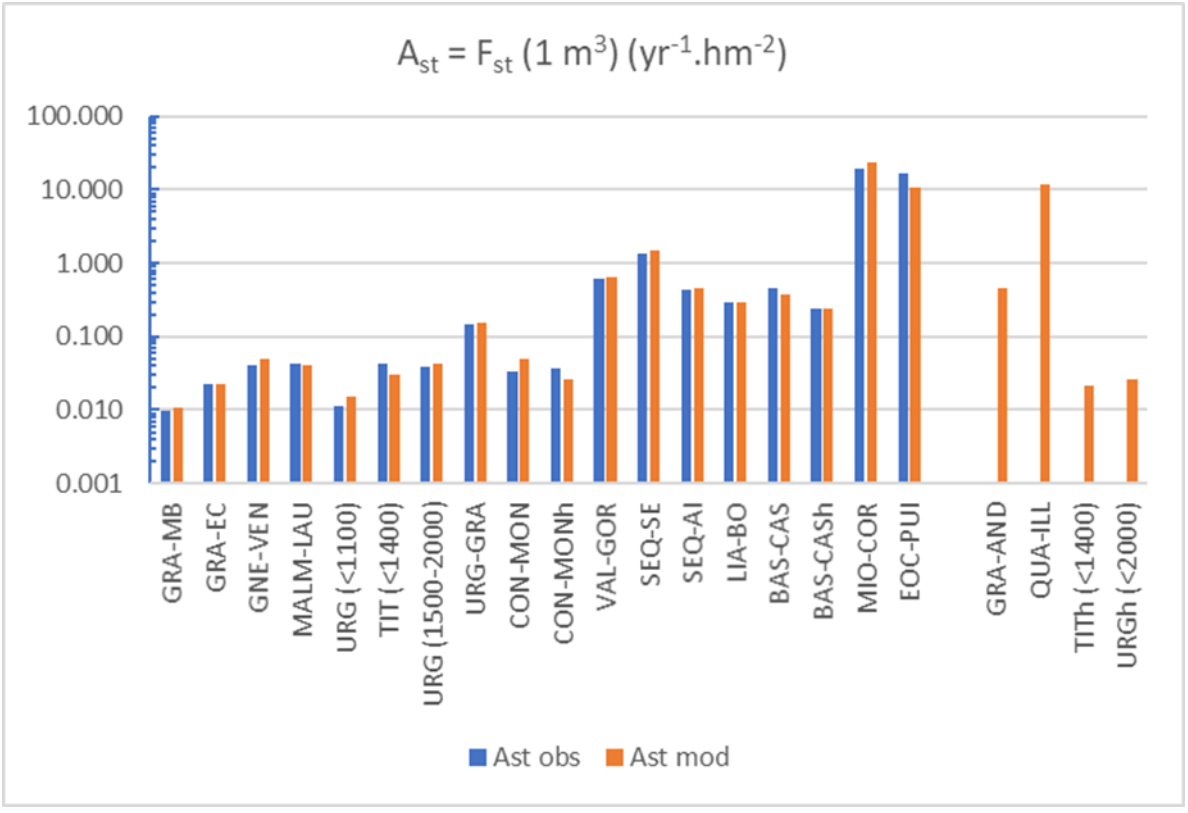

Figure 4: Observed ($A_{st\ obs}$) and modelled ($A_{st\ mod}$) spatio-temporal frequency of failures larger than 1 m^3 expressed in $yr^{-1}.hm^{-2}$ for the sites reviewed in this study.

5 Discussion

5.1 Observed frequency

Tables 3 and 4 and Figure 4 show that the highest values of A_{st} (around 10 $yr^{-1}.hm^{-2}$) occur for MIO-COR, EOC-PUI and QUA-ILL. MIO-COR and EOC-PUI are cliffs composed of alternating hard and weak beds and form the scarp of landslides. QUA-ILL is located above a very active catchment prone to debris flows. This highlights the importance of the geomorphological context and the heterogeneity of the cliff.

Aside from these cliffs, a second level of analysis allows to distinguish two groups corresponding respectively to intervals [0.01-0.1] and [0.1-1]. The first group includes cliffs consisting of massive hard rock (joint spacing frequently larger than 2 m, high compressive strength). The URG-GRA cliff is an exception that will be discussed later. The second group includes cliffs consisting of hard rock with joint spacing smaller than 2 m.

In order to classify the cliffs according to their failure frequency, three groups of cliffs can be distinguished in accordance with the ISRM description of the joint spacing (Table 5): Spacing > 2 m; spacing between 0.6 and 2 m; and spacing between 0.2

https://doi.org/10.5194/egusphere-2025-6247
Preprint. Discussion started: 22 December 2025

and 0.6 m. Note estimating a significant joint spacing in sedimentary rocks can be challenging, because visible bedding joints can have considerable cohesion or include rock bridges.

The cliffs of the first group made up of massive hard rock are usually very high and steep cliffs, and release very large blocks. In the French Urgonian limestone cliffs, we observed deposited blocks of several hundred cubic metres (up to 1000 m^3). Ruiz-Carulla et al. (2020) also observed blocks of several hundred cubic metres in massive Mesozoic limestone in Spain (joint spacing > 3 m). As it may be difficult to determine the joint spacing, the largest observed block volumes can help to classify a cliff in this group (Table 5). Note that to determine the largest possible block volume, a large area must be observed; therefore, it may be useful to consider other cliffs with similar geological features. We also suggest that rock cliffs that are qualified as very good in the RMR classification (Bieniawski, 1989) should belong to this group. Practically, this means that tunnelling in these rocks usually does not require systematic support. Note that the studied limestone cliffs are anaclinal slopes with a favourable orientation that does not need a rating adjustment for discontinuity orientation. These rocks are described as good rock by climbers and can support long, popular, multi-pitch climbing routes. Mont Granier is an exception in this group, with a frequency of 0.15 $yr^{-1}.hm^{-2}$, due to the cliff being part of a huge rock avalanche scar (500 hm^3) that occurred in 1248 – one of the largest scars observed in the European Alps in the last millennium.

According to our classification, the frequency of the second group (0.6 to 2 m) is expected to be lower than that of the third group (0.2 to 0.6 m). However, this is not supported by the two cliffs of this study that belong to the second group, which show frequencies similar to those in the third group (0.2 to 20 $yr^{-1}.hm^{-2}$). This discrepancy can most likely be explained by the fact that the only two cliffs of group 2 (VAL-GOR and MIO-COR) are located above active erosion gullies, a geomorphological context that is likely to significantly increase the failure frequency.

Table 5: Spatio-temporal frequency A_{st} ($yr^{-1}.hm^{-2}$) of failures larger than 1 m^3 according to the geomorphological context of the cliff and the joint spacing or the maximal possible block volume. Last column: exponent B of the volume–frequency relationship.

Group	Joint spacing (m)	Maximal possible block volume (m^3)	Ast (cliff above a stable slope)	Ast (cliff above an active landslide or gully)	B
1	>2	Hundreds of m^3	0.01-0.1	0.1-1	0.5±0.2
2	0.6-2	Tens of m^3	0.05-0.5	0.5-5	0.6±0.25
3	0.2-0.6	Some m^3	0.2-2	2-20	0.7±0.3

Using some of the cliffs from the study, Hantz et al. (2020) highlighted the influence of joint spacing (S) on A_{st} and proposed an approximative relationship to quantify this influence:

$$A_{st} = 10^{-\log(10S)} = 0.1S^{-1} \quad (9)$$

To refine this relationship, we fitted a power law to the frequencies observed in cliffs located above a stable area. Since the uncertainty on A_{st} varies across cliffs, we cannot apply the standard linear regression method, which assumes identical uncertainties. The uncertainty on A_{st} was roughly modelled with a normal distribution, with mean equal to $A_{st\,obs}$ and standard

https://doi.org/10.5194/egusphere-2025-6247
Preprint. Discussion started: 22 December 2025

deviation approximated by ($A_{st\ max}$ - $A_{st\ min}$)/4, and the uncertainty on S was modelled with a rectangular distribution defined from different spacing intervals (0.8 S_{min} to 1.2 S_{max}). For each cliff, 1000 Monte-Carlo simulations were drawn and a linear regression made (Fig. 5). The resulting relationship is:

$$A_{st} = 0.27S^{-1.19} \quad (10)$$

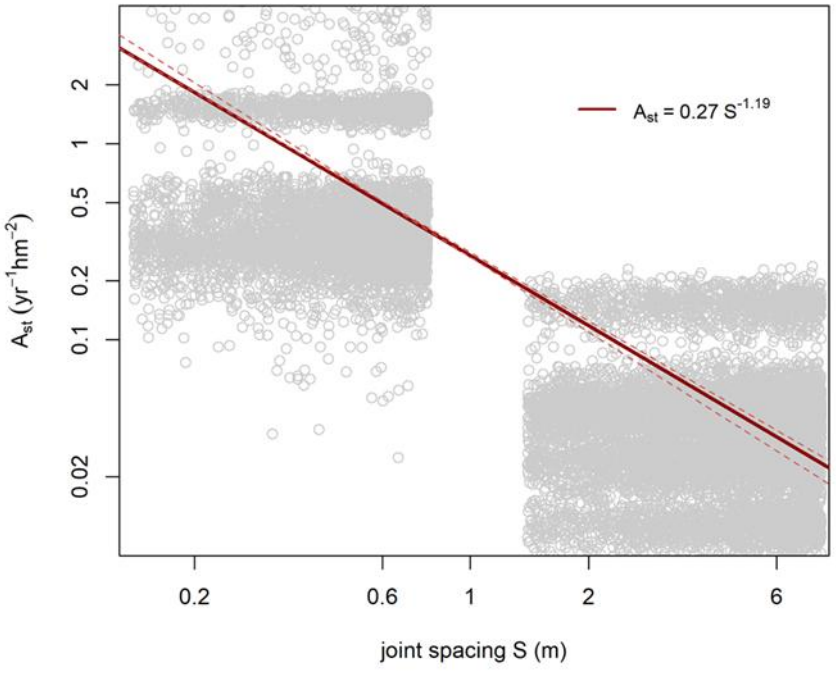

Figure 5: Relationship between the spatio-temporal failure frequency A_{st} (y-axis) and the joint spacing for the cliffs above a stable slope, using a Monte-Carlo simulation.

In addition to the joint spacing, our study suggests that the failure frequency for cliffs over a stable slope is further influenced by the elevation and heterogeneity of the cliff. These factors could explain that some upper limits of the frequency (Table 3) are higher than the intervals given in Table 5. The Urgonian cliffs, at an altitude of 1500–2000 m, have a frequency3.7 times higher than those at lower elevation. It appears that the higher the elevation, the higher the frequency. This altitude influence can be explained by the increase in precipitation and the number of freeze-thaw cycles with altitude (under 2000 m, for the range of latitudes considered). Indeed, several studies showed that these factors can increase the failure frequency (e.g., D'Amato et al., 2016; Pratt et al., 2019; Lowe et al., 2022; Mainieri et al., 2023).

The La Cornalle cliff and Gorgette cliff have similar joint spacing and are both located above an unstable slope, but the former has a frequency 31 times higher than the latter. We suggest that the strong heterogeneity and presence of marl in La Cornalle explains this difference. Wyllie (2017) noted that bedded sedimentary formations, which consist of weak rocks prone to weathering and stronger rocks, are often prone to rockfalls. Differential weathering is an important factor in the well-known

https://doi.org/10.5194/egusphere-2025-6247
Preprint. Discussion started: 22 December 2025

Rockfall Hazard Rating System (as well as precipitation and freezing). It is suggested that the values in Table 5 can be increased in cases of differential weathering.

Schneider et al. (2023) monitored (with a Doppler radar) a dolomite cliff in a very active rockslide complex that moved more than 10 $m.yr^{-1}$ in Brienz/Brinzauls (Switzerland). In this particular geomorphological context, not observed in the studied sites, they found a failure frequency of the order of 100 $yr^{-1}.hm^{-2}$.

Note that there is no group of cliffs made up of rock with joint spacing smaller than 0.2 m. It seems that this type of rock cannot constitute high (tens of meters) and steep natural cliffs, but rather more gentle slopes that are often forested, ravined or covered with scree, under the climatic and geomorphological conditions considered in this study.

5.2 Frequency derived from the power law model

Table 4 and Figure 5 show a good correlation between the observed frequency and the frequency derived from the power law model (the ratio varies between 0.65 and 1.46). Thus, the cliffs for which the frequency of failures larger than 1 m^3 was estimated by extrapolation of the power law were included in the analysis. Their failure frequencies are compatible with the proposed classification (Tables 3, 4; Fig. 4).

5.3. Frequency estimated by expert judgement

When no exhaustive inventory is available, the frequency is usually estimated by expert judgement from available information. Agliardi et al. (2009) estimated rockfall frequency from historical and geomorphological information, in a cliff consisting of massive or thick-bedded Middle Triassic dolostones, located in the Central Southern Alps in Italy. The frequency of failures larger than 1 m^3 is about 0.05 $yr^{-1}.hm^{-2}$. Corominas et al. (2019) estimated rockfall frequency from historical records and the number of rock blocks intercepted by barriers under a massive limestone and dolostone cliff, of Upper Cretaceous age, located in Spain. The frequency of failures larger than 1 m^3 is about 0.01 $yr^{-1}.hm^{-2}$. Both estimations are consistent with the proposed classification.

5.4. Frequency estimated from deposited blocks

Farvacque et al. (2022) counted deposited blocks and recorded tree growth over a 24-year period beneath a cliff composed of highly fractured granite, gneiss and schist in La Fory (Switzerland) at altitudes between 700 m and 1300 m. Using a propagation model, they calculated a block release frequency in the order of 1 $yr^{-1}.hm^{-2}$ for blocks bigger than 0.5 m^3. A failure usually releases several individual blocks that can break during impact, so this value can be considered as an upper limit of the failure frequency. This corresponds to the scenario where all failures result in the fall of a unique block that does not break. Because the years are known when growth disturbances occurred, a lower limit can be estimated by assuming that all disturbances in the same pathway happened in the same year as the result of a unique rockfall event. Assuming this scenario, the 35 and 41 disturbances observed in plots C1 and C3, respectively, over 24 years are the result of 10 and 17 rockfall events. The mean number of blocks per event would be 3.5 and 2.4, respectively. So, the upper limit of the failure frequency (scenario 1) must

https://doi.org/10.5194/egusphere-2025-6247
Preprint. Discussion started: 22 December 2025

be divided by about three to obtain the lower limit (scenario 2), which is of the order of 0.3 $yr^{-1}.hm^{-2}$. According to the power law, the frequency of failures bigger than 1 m^3 is obtained by dividing the frequency of failures bigger than 0.5 m^3 by 2^{-B}. Considering that La Fory cliff belongs to group 2 or 3 (Table 5), B is around 0.65, and then the lower and upper limit for A_{st} are 0.2 and 0.6 $yr^{-1}.hm^{-2}$, respectively. These values are consistent with group 2 or 3 and align with the description "highly fractured". Among the cliffs analysed in this study, the cliff in Andorra, made of highly fractured granodiorite and hornfels, has characteristics close to those of La Fory and a failure frequency of 0.45 $yr^{-1}.hm^{-2}$, which situates it also in group 2 or 3.

5.5. Comparison with the meta-analysis by Phillips and Walton (2025)

Phillips and Walton (2025) used 44 rockfall inventories to analyse some factors influencing rockfall activity: geological, climatic and database (non-physical) variables. Unlike this study, the activity of the slope under the cliff was not considered. Out of the 44 inventories, 14 are in the scope of our study (natural non-coastal rock walls located in temperate climate zones and below the permafrost area, deposited blocks not considered) and 11 are common with our study. Despite some differences in the methods used, the values of A_{st} obtained by Phillips and Walton are close to our values. They found that rock mass condition (the amount of rock fracturing) and geology are the most relevant geological variables for characterising rockfall activity. All bedded sedimentary cliffs (bedding spacing less than 1 m or rock layers of variable strength) have A_{st} bigger than 1 $yr^{-1}.hm^{-2}$ and most massive sedimentary cliffs (bedding spacing larger than 1 m) have A_{st} lower than 1 $yr^{-1}.hm^{-2}$. The median values differ by more than one order of magnitude (Phillips and Walton, 2025, Fig. 11). Their results are consistent with our results. They also found that a natural or a cut slope has a strong effect on rockfall activity, likely due to a combination of blast-induced damage, stress relaxation and over-steepening of the slope beyond the natural stable angle.

5.6. Practical hazard level

In order to exemplify the practical meaning of the failure frequency, Table 6 shows the passage frequency of rockfalls at the foot of three cliffs of different height (10, 100 and 1000 m). In these examples, the failure frequencies of the three cliffs were chosen so that they produce the same passage frequency at the foot. This passage frequency can be used to quantify the hazard for a road running along the base, expressed as the annual number of rockfalls per unit length of the cliff. Table 6 also shows the corresponding qualitative descriptors according to Fell et al. (2008). A propagation analysis can be used to determine the passage frequency at locations further downslope from the cliff. Without fragmentation, the passage frequency decreases along the slope as blocks stop. But if fragmentation occurs, the passage frequency may increase near the foot of the cliff, with fragments of smaller volume and energy (Corominas et al., 2019).

https://doi.org/10.5194/egusphere-2025-6247
Preprint. Discussion started: 22 December 2025

Table 6. Passage frequency at the cliffs' base, according to the failure frequency for different cliff heights. Qualitative descriptors according to Fell et al. (2008).

Failure frequency for	unit					
Height = 10 m	$yr^{-1}.hm^{-2}$	> 10	1 to 10	0.1 to 1	0.01 to 0.1	< 0.01
Height = 100 m	$yr^{-1}.hm^{-2}$	> 1	0.1 to 1	0.01 to 0.1	0.001 to 0.01	< 0.001
Height = 1000 m	$yr^{-1}.hm^{-2}$	> 0.1	0.01 to 0.1	0.001 to 0.01	0.0001 to 0.001	< 0.0001
Passage frequency at cliff foot	$yr^{-1}.hm^{-1}$	> 1	0.1 to 1	0.01 to 0.1	0.001 to 0.01	< 0.001
Qualitative descriptor at cliff foot		Very high	High	Moderate	Low	Very low

5.7. Methods to estimate the failure frequency

Depending on the available information, the failure volume–frequency relationship can be determined by different methods, as shown in Table 7. When an exhaustive inventory is available, with a sufficient number of events for a significant power law fitting, the two parameters of the power law (A_{st} and B) can be determined along with their uncertainties (e.g., Van Veen et al., 2017; Guerin et al., 2020; Hantz et al., 2020a). Note that the power law is valid only for the observed volume range. If the number of events is insufficient for a significant power law fitting, the method proposed here allows estimation of a confidence interval for A_{st} , while B (if needed) can be roughly estimated using the classification proposed in Table 5. When no exhaustive inventory is available, both parameters must be estimated using either this classification or the relationship between A_{st} and S (Fig. 5). In the latter two cases, B can be estimated by power law fitting using rockfall scars and/or potentially unstable blocks.

Table 7. Methods to determine volume–frequency relationship parameters.

Data available	A_{st}	B
Exhaustive inventory with many events	Power law fitting	Power law fitting
Exhaustive inventory with few events	Confidence interval using Poisson's law	Classification
No exhaustive inventory	Classification / relation between A_{st} and joint spacing S	Classification

5.8. Uniformity parameter (power law exponent)

The value of the uniformity parameter B has a particular importance when extrapolation is used to estimate the frequency of failures larger (or smaller) than the volume range of observations. When a power law fitting is insignificant, an estimation of B, based on the characteristics of the cliff, is proposed. Considering a data set from French cliffs with rockfall volumes lower

https://doi.org/10.5194/egusphere-2025-6247
Preprint. Discussion started: 22 December 2025

than 1000 m^3, Hantz and Levy (2019) and Hantz et al. (2020a) found that B was lower for massive rock masses than for thinly bedded ones.

The values of B for the different cliffs are given in Table 4. They vary between 0.32 and 0.81 for group 1, between 0.56 and 0.65 for group 2 (only two cliffs) and between 0.44 and 1.01 for group 3. The volume range giving the B value of 0.81 in group 1 is the only one entirely under 1 m^3. Janeras et al. (2023) suggested that the B value could depend on the failure mechanism. Values around 0.8 correspond to a mechanism (mec3) in which pebbles detach from the conglomerate due to matrix weathering but remain resistant, resulting in release volumes smaller than 0.1 m^3. Larger failure volumes correspond to two other mechanisms (mec2 and mec1). Mec2 involves weathering flakes produced by thermal exfoliation, while mec1 corresponds to failures delimited by mechanical discontinuities in the rock mass. For these two mechanisms, the authors found B values of 0.6 and 0.4, respectively. This difference is illustrated by two samples (as seen in Table 2): CON-MON is obtained by TLS monitoring with high precision and limited sampling extent (collecting activity mainly from mec3 and some from mec2), while CON-MONh is obtained by observational and historical inventories covering a large sampling extent, but able to detect only larger rockfalls (mec 2 and mec1). If the smallest volumes corresponding to the mec3 mechanism in Montserrat are excluded, the range of B values for group 1 is between 0.32 and 0.7.

The relationship between B and the joint spacing is less clear than that found by Hantz and Levy (2019); however, it should be noted that the range of B values for massive rocks (0.32 to 0.7) is lower than for more jointed ones (0.44 to 1.01). This can be explained by the fact that small failures are more probable in more jointed rocks (inducing higher values for B). For example, large overhangs can appear in massive rocks and produce large failures. In more jointed rocks, overhang toppling occurs with higher frequency for smaller overhangs. Suggested B values for the three groups are given in Table 5. More inventories are needed to accurately analyse the factors that influence B, and a better estimation of the joint spacing is needed for a more precise classification.

Note that historical inventories of large rockfall events for several cliffs (like TITh and URGh) can give a higher B value than the B values estimated for each cliff, if the heights of the cliffs are different. This can be due to the following reason: The volume at which the power law must be truncated (maximum possible volume, V_{MAX}) depends mainly on the height of the cliff. If the cliff heights are equal, the maximum possible volumes are equal, and the sum of the frequency distributions (truncated power laws) follows a truncated power law with the same B value. But if the cliff heights are different (Fig. 6), the maximum possible volumes are different, and the sum of the frequency distributions (truncated power laws) is not a power law. When the volume exceeds the lowest V_{MAX}, the distribution function decreases in steps, corresponding to the V_{MAX} values of the different cliffs. This theoretical shape is usually not visible because of the low number of large failures, and a power law fitting leads to B values higher than the B values of the individual cliffs (Fig. 6). This was observed by Hantz and Levy (2019) for French Urgonian cliffs: The B value for the historical inventory of large failures (larger than 1000 m^3) of many cliffs, with heights varying from tens of metres to hundreds of metres, is 0.7, whereas the TLS inventories of smaller failures (smaller than 1000 m^3) that occurred in three cliffs gave B values between 0.3 and 0.5. In a similar sense, Janeras et al. (2023) proposed to consider and compute sampling extent dependent on the considered volume.

https://doi.org/10.5194/egusphere-2025-6247
Preprint. Discussion started: 22 December 2025

Graber and Santi (2022) also studied the factors that influence the exponent of the power law, but they considered the probability density function (PDF) instead of the cumulative frequency. Their exponent "b" = B+1. They obtained b values ranging between 1.2 and 2.6, which correspond to B values between 0.2 and 1.6, instead of 0.3 to 1.0 in our study. However, they combined inventories of failures with inventories of individual blocks (i.e., fragments of failures deposited on the slope), which usually have larger B values (Hantz et al., 2020a). Without considering the inventories of fragments, the range of B values is comparable to the range reported here, which rarely exceeded 1. Contrary to our result, they found higher b values associated with higher-quality rock masses, but with a low significance level (p = 0.056). With a higher significance level (p = 0.03), higher B values were associated with smaller maximum rockfall volumes of the inventory. This result is consistent with our suggestion that higher B values are associated with lower joint spacing.

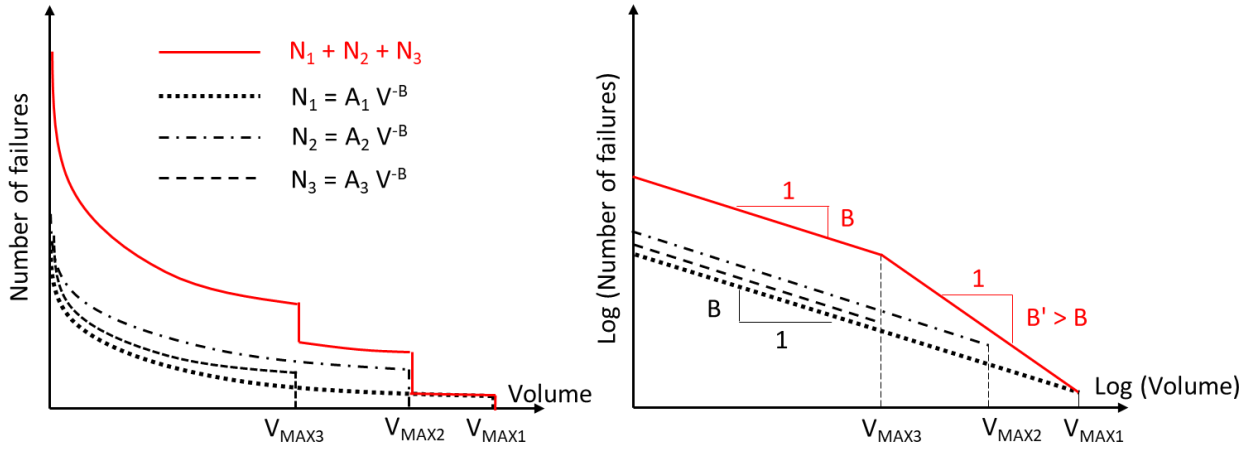

Figure 6: Cumulated distribution functions (CDF N_1, N_2, N_3) for three cliffs of different height and maximum possible failure volumes (V_{MAX1}, V_{MAX2}, V_{MAX3}) and CDF when these cliffs are considered together ($N_1+N_2+N_3$). For V > V_{max3}, the slope of the red curves increases and power law fitting gives a higher exponent.

5.9. Influence of the uncertainty about B

When the volume of interest is not in the volume interval covered by the inventory (it may be smaller or larger), an extrapolation is possible, assuming the power law is valid up to this volume. But the uncertainty about the parameter B (De Biagi, 2017) leads to uncertainty about the interpolated frequency. Table 8 shows an example where the frequency of failures larger than 1 m^3 was estimated to 1 $yr^{-1}.hm^{-2}$ and is extrapolated using a power law with different values of B. As the hazard descriptors (for passage frequency and consequently for failure frequency) are based on the decimal logarithm of the frequency, we consider an uncertainty of log (F_{st}) lower than 0.5 as acceptable. It therefore follows that extrapolation from 1 m^3 to 100 m^3 (two orders of magnitude) is acceptable for the cliffs in group 1 (B = 0.5±0.2). For group 2 and 3 cliffs, extrapolation is acceptable only from 1 m^3 to 10 m^3 (one order of magnitude).

https://doi.org/10.5194/egusphere-2025-6247
Preprint. Discussion started: 22 December 2025

Table 8. Extrapolated failure frequency ($yr^{-1}.hm^{-2}$) for different minimum volumes and different B values, in a cliff where the frequency of failures larger than 1 m^3 (A_{st}) is equal to 1 $yr^{-1}.hm^{-2}$.

V (m^3)	1	10	100	1000	10000	100000
B	F_{st} (V)	F_{st} (V)	F_{st} (V)	F_{st} (V)	F_{st} (V)	F_{st} (V)
0.3	1	0.50	0.25	0.126	0.0631	0.03162
0.4	1	0.40	0.16	0.063	0.0251	0.01000
0.5	1	0.32	0.10	0.032	0.0100	0.00316
0.6	1	0.25	0.06	0.016	0.0040	0.00100
0.7	1	0.20	0.04	0.008	0.0016	0.00032
0.9	1	0.13	0.02	0.002	0.0003	0.00003
1	1	0.10	0.01	0.001	0.0001	0.00001

5.10. Rockfall activity

A complete description of rockfall activity requires knowledge of both A_{st} and B parameters. Figure 7 shows the volume–frequency relationship for exemplary cliffs of groups 1 and 3, with the mean values of A_{st} and B given in Table 5. The frequency of failures larger than 1 m^3 in group 3 is significantly higher than in group 1, but for volumes larger than 1000 m^3 the frequency is higher in group 1. Cliffs cannot be ranked according to a level of activity if we consider the full range of possible volumes; however, the consequences of the different volume scenarios can be integrated into risk analyses.

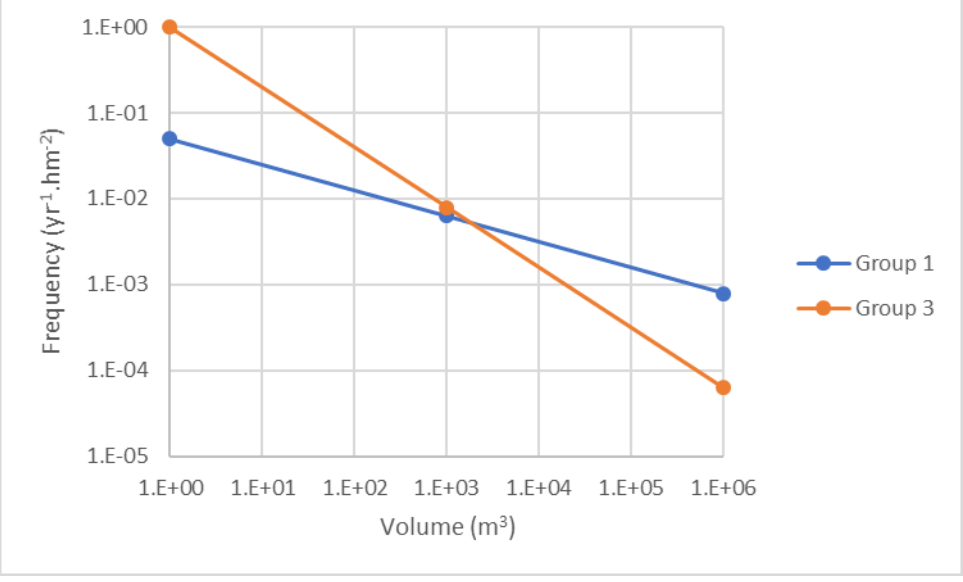

Figure 7: Frequency as a function of the failure volume for typical cliffs in groups 1 and 3 (defined in Table 5).

5.11. Joint spacing

https://doi.org/10.5194/egusphere-2025-6247
Preprint. Discussion started: 22 December 2025

Priest and Hudson (1981) showed that joint spacing follows, in most cases, a negative exponential distribution. This means that the most commonly occurring joints are closely spaced and, consequently, they strongly influence the mean spacing. But they are often concentrated in highly jointed zones that are not representative of the whole rock mass and that release small rockfalls. To estimate the failure frequency of rockfalls larger than 1 m^3, we propose to quantify the zones where joints are widely spaced. Following the principle of the Rock Quality Designation (RQD) used for tunnel design, the percentage of a cliff height, where the spacing is higher than 1 m (instead of 0.1 m for the RQD), can be considered. Inversely, the spacing S_{50}, for which 50% of the height of the cliff has spacings larger than S_{50}, can be determined.

The identification of significant joints remains difficult. Ideally, only discontinuity surfaces with zero or very low tensile strength ("mechanical" joints) should be considered for estimating the joint spacing; this excludes certain discontinuities. A "mechanical" spacing could be estimated from the observation of overhangs, because the possible length of a cantilever bed increases with bed thickness (Kogure et al., 2006).

6. Conclusions and perspectives

This study proposes a new method to estimate a confidence interval for the frequency of failures exceeding a given volume, even when the available exhaustive inventory contains only a few, or no, events. For cases where the volume–frequency relationship can be fitted with a power law, the frequencies obtained by the two methods are similar.

The meta-analysis of 22 inventories of failures in natural mountain cliffs located in temperate climates and under the permafrost limit shows that the main factors influencing the spatio-temporal failure frequency are activity of the underlying slope, homogeneity of the cliff, joint spacing, and altitude. The frequency of failures bigger than 1 m^3 varies by at least three orders of magnitude, from 0.01 to 20 $yr^{-1}.hm^{-2}$. The exponent of the power law varies between 0.3 and 1.0 and tends to be lower for massive rock than for bedded rock.

A primary cliff classification is proposed to estimate the order of magnitude for the frequency of failures larger than 1 m^3 and the exponent of the power law. The provided guiding values are only tested in the selected context (natural slopes, low-altitude, mid-latitude, temperate climate). This can serve as an important basis for the derivation and validation of rockfall release scenarios for diffuse hazards with limited data on past events. The estimation of the parameters of the volume–frequency relationship can also be made by comparing pictures of cliffs to those of our study sites (shown in the supplement).

More inventories are needed to enhance the proposed classification. Additionally, other geomorphological and geological contexts could be included in the analysis, including rock walls in the permafrost zone, coastal and riverbank cliffs, or man-made cut slopes. Generally, the current literature indicates that failure frequencies in those cliffs are largely higher than in the natural cliffs considered in this study (e.g., Hantz et al., 2020a).

https://doi.org/10.5194/egusphere-2025-6247
Preprint. Discussion started: 22 December 2025

Author contributions

This research was conceptualized by D. Hantz, M. Jaboyedoff, C. Moos, L. Dorren. All authors contribute to formal analysis, methodology, writing and review.

Competing interests

The authors declare that they have no conflict of interest.

Acknowledgements

This work was partly supported by the research project C2ROP. We would like to thank Angela Wade for proofreading our manuscript.

References

Abellán, A., Calvet, J., Vilaplana, J. M., and Blanchard, J.: Detection and spatial prediction of rockfalls by means of terrestrial laser scanner monitoring, Geomorphology, 119, 162–171, https://doi.org/10.1016/j.geomorph.2010.03.016, 2010.

Abellán, A., Vilaplana, J. M., Calvet, J., García-Sellés, D., and Asensio, E.: Rockfall monitoring by Terrestrial Laser Scanning – case study of the basaltic rock face at Castellfollit de la Roca (Catalonia, Spain), Nat. Hazards Earth Syst. Sci., 11, 829–841, https://doi.org/10.5194/nhess-11-829-2011, 2011.

Agliardi, F., Crosta, G. B., and Frattini, P.: Integrating rockfall risk assessment and countermeasure design by 3D modelling techniques, Nat. Hazards Earth Syst. Sci., 9, 1059–1073, https://doi.org/10.5194/nhess-9-1059-2009, 2009.

Alber, S.: Change detection combining SfM and LiDAR techniques: Application to the study of rockfalls using archival photographs, Katholische Universität Eichstätt-Ingolstadt, Université de Lausanne, 2016.

Bennett, G. L., Molnar, P., Eisenbeiss, H., and McArdell, B. W.: Erosional power in the Swiss Alps: characterization of slope failure in the Illgraben: EROSIONAL POWER IN THE SWISS ALPS: SLOPE FAILURE IN THE ILLGRABEN, Earth Surf. Process. Landforms, 37, 1627–1640, https://doi.org/10.1002/esp.3263, 2012.

Bieniawski, Z. T.: Engineering rock mass classifications: a complete manual for engineers and geologists in mining, civil, and petroleum engineering, Wiley, New York, 251 pp., 1989.

Blanch, X.: Anàlisi de l'evolució de despreniments a partir de dades LiDAR a l'escarpament de Puigcercós (Pallars Jussà), https://doi.org/10.13140/RG.2.2.17912.37123, 2015.

Bourrier, F., Dorren, L., and Hungr, O.: The use of ballistic trajectory and granular flow models in predicting rockfall propagation, Earth Surf Processes Landf, 38, 435–440, https://doi.org/10.1002/esp.3372, 2013.

https://doi.org/10.5194/egusphere-2025-6247
Preprint. Discussion started: 22 December 2025

Carrea, D., Abellan, A., Derron, M.-H., Gauvin, N., and Jaboyedoff, M.: MATLAB Virtual Toolbox for Retrospective Rockfall Source Detection and Volume Estimation Using 3D Point Clouds: A Case Study of a Subalpine Molasse Cliff, Geosciences, 11, 75, https://doi.org/10.3390/geosciences11020075, 2021.

Corominas, J., Matas, G., and Ruiz-Carulla, R.: Quantitative analysis of risk from fragmental rockfalls, Landslides, 16, 5–21, https://doi.org/10.1007/s10346-018-1087-9, 2019.

Corominas, J., Mavrouli, O., and Ruiz-Carulla, R.: Magnitude and frequency relations: are there geological constraints to the rockfall size?, Landslides, 15, 829–845, https://doi.org/10.1007/s10346-017-0910-z, 2018.

Corominas, J., van Westen, C., Frattini, P., Cascini, L., Malet, J.-P., Fotopoulou, S., Catani, F., Van Den Eeckhaut, M., Mavrouli, O., Agliardi, F., Pitilakis, K., Winter, M. G., Pastor, M., Ferlisi, S., Tofani, V., Hervás, J., and Smith, J. T.: Recommendations for the quantitative analysis of landslide risk, Bulletin of Engineering Geology and the Environment, 73, 209–263, https://doi.org/10.1007/s10064-013-0538-8, 2014.

D'Amato, J.: Apport d'une base de données d'éboulements rocheux obtenue par scanner laser dans la caractérisation des conditions de rupture et processus associés, Université Grenoble Alpes, https://theses.fr/2015GREAU025, 2015.

D'Amato, J., Hantz, D., Guerin, A., Jaboyedoff, M., Baillet, L., and Mariscal, A.: Influence of meteorological factors on rockfall occurrence in a middle mountain limestone cliff, Nat. Hazards Earth Syst. Sci., 16, 719–735, https://doi.org/10.5194/nhess-16-719-2016, 2016.

De Biagi, V.: Brief communication: Accuracy of the fallen blocks volume-frequency law, Nat. Hazards Earth Syst. Sci., 17, 1487–1492, https://doi.org/10.5194/nhess-17-1487-2017, 2017.

De Biagi, V., Napoli, M. L., Barbero, M., and Peila, D.: Estimation of the return period of rockfall blocks according to their size, Nat. Hazards Earth Syst. Sci., 17, 103–113, https://doi.org/10.5194/nhess-17-103-2017, 2017.

Dorren, L., Berger, F., Bourrier, F., Eckert, N., Saroglou, C., Schwarz, M., Stoffel, M., Trappmann, D., Utelli, H.-H., and Moos, C.: Delimiting rockfall runout zones using reach probability values simulated with a Monte-Carlo based 3D trajectory model, Natural Hazards and Earth System Sciences Discussions, 2022, 1–23, https://doi.org/10.5194/nhess-2022-32, 2022.

Durville, J. L.: Quelques remarques sur l'emploi des probabilites dans le domaine des risques naturels : Cas des mouvements de terrain, https://api.semanticscholar.org/CorpusID:127014351, 2004.

Dussauge-Peisser, C., Helmstetter, A., Grasso, J.-R., Hantz, D., Desvarreux, P., Jeannin, M., and Giraud, A.: Probabilistic approach to rock fall hazard assessment: potential of historical data analysis, Nat. Hazards Earth Syst. Sci., 2, 15–26, https://doi.org/10.5194/nhess-2-15-2002, 2002.

Epinat, C.: Evaluation quantitative de l'aléa d'éboulement rocheux par acquisitions Lidar sur 4 falaises de la région grenobloise, Université Grenoble Alpes (Polytech, ISTerre), Université de Lausanne, 2016.

Farvacque, M., Corona, C., Lopez-Saez, J., Mainieri, R., Stoffel, M., Bourrier, F., Eckert, N., and Toe, D.: Estimating rockfall release frequency from blocks deposited in protection barriers, growth disturbances in trees, and trajectory simulations, Landslides, 19, 7–18, https://doi.org/10.1007/s10346-021-01719-0, 2022.

https://doi.org/10.5194/egusphere-2025-6247
Preprint. Discussion started: 22 December 2025

Fell, R., Corominas, J., Bonnard, C., Cascini, L., Leroi, E., and Savage, W. Z.: Guidelines for landslide susceptibility, hazard and risk zoning for land use planning, Engineering Geology, 102, 85–98, https://doi.org/10.1016/j.enggeo.2008.03.022, 2008.

Graber, A. and Santi, P.: Power law models for rockfall frequency-magnitude distributions: review and identification of factors that influence the scaling exponent, Geomorphology, 418, 108463, https://doi.org/10.1016/j.geomorph.2022.108463, 2022.

Guerin, A., Rossetti, J.-P., Hantz, D., and Jaboyedoff, M.: Estimating rockfall frequency in a mountain limestone cliff using terrestrial laser scanner, Univ. Grenoble Alpes, Univ. Savoie Mont Blanc, CNRS, IRD, Univ. Gustave Eiffel, ISTerre, France; Université de Lausanne, Switzerland, 2013. https://insu.hal.science/insu-03598668

Guerin, A., Stock, G. M., Radue, M. J., Jaboyedoff, M., Collins, B. D., Matasci, B., Avdievitch, N., and Derron, M.-H.: Quantifying 40 years of rockfall activity in Yosemite Valley with historical Structure-from-Motion photogrammetry and terrestrial laser scanning, Geomorphology, 356, 107069, https://doi.org/10.1016/j.geomorph.2020.107069, 2020.

Guillemot, A.: Évaluation quantitative de l'aléa de départ des éboulements rocheux, Ecole Polytechnique Fédérale de Lausanne, Université Grenoble Alpes (Laboratoire ISTerre), https://infoscience.epfl.ch/entities/publication/3dd4c310-2505-42e4-94b3-9d66e0d0586b, 2017.

Hantz, D., Colas, B., Dewez, T., Lévy, C., Rossetti, J.-P., Guerin, A., and Jaboyedoff, M.: Caractérisation quantitative des aléas rocheux de départ diffus (Quantitative assessment of rockfall release frequency), Rev. Fr. Geotech., 2, https://doi.org/10.1051/geotech/2020011, 2020a.

Hantz, D., Colas, B., Dewez, T., Levy, C., Rossetti, J.-P., Guerin, A., and Jaboyedoff, M.: Caractérisation quantitative des aléas de départ diffus, Projet National C2ROP, LC/19/C2ROP/282, 2020b.

Hantz, D., Corominas, J., Crosta, G. B., and Jaboyedoff, M.: Definitions and Concepts for Quantitative Rockfall Hazard and Risk Analysis, Geosciences, 11, 158, https://doi.org/10.3390/geosciences11040158, 2021.

Hantz, D., Jaboyedoff, M., Moos, C., and Dorren, L.: Failure frequency in some types of rock walls, in: 14TH INTERNATIONAL SYMPOSIUM ON LANDSLIDES, Chambéry, 304–307, ISBN 978-2-9585706-1-3, 2024.

Hantz, D. and Levy, C.: Quantification de l'aléa diffus (Diffuse hazard quantification), Projet National C2ROP, LC/16/C2ROP/93, 2019.

Hantz, D., Dussauge-Peisser, C., Jeannin, M., and Vengeon, J.-M.: Rock fall hazard assessment: from qualitative to quantitative failure probability, in: Fast Slope Movements, Int. Conf. on Fast Slope Movements, Naples, 263–267, 2003.

Hoek, E. and Bray, J.: Rock slope engineering, 3. rev. ed., reprinted., E & FN Spon, London, 358 pp., 2001.

Hungr, O., Evans, S. G., and Hazzard, J.: Magnitude and frequency of rock falls and rock slides along the main transportation corridors of southwestern British Columbia, Can. Geotech. J., 36, 224–238, https://doi.org/10.1139/t98-106, 1999.

Hungr, O., Leroueil, S., and Picarelli, L.: The Varnes classification of landslide types, an update, Landslides, 11, 167–194, https://doi.org/10.1007/s10346-013-0436-y, 2014.

https://doi.org/10.5194/egusphere-2025-6247
Preprint. Discussion started: 22 December 2025

ISRM: International Society for Rock Mechanics, Commission on Classification of Rocks and Rock Masses, Basic geotechnical description of rock masses, International Journal of Rock Mechanics and Mining Sciences & Geomechanics Abstracts, 18, 85–110, https://doi.org/10.1016/0148-9062(81)90277-1, 1981.

Jaboyedoff, M., Ben Hammouda, M., Derron, M.-H., Guerin, A., Hantz, D., and Noel, F.: The rockfall failure hazard assessment: Summary and new advances, in: Understanding and reducing landslide disaster risk, Kyoto, 2020.

Janeras, M., Jara, J.-A., Royán, M. J., Vilaplana, J.-M., Aguasca, A., Fàbregas, X., Gili, J. A., and Buxó, P.: Multi-technique approach to rockfall monitoring in the Montserrat massif (Catalonia, NE Spain), Engineering Geology, 219, 4–20, https://doi.org/10.1016/j.enggeo.2016.12.010, 2017.

Janeras, M., Lantada, N., Núñez-Andrés, M. A., Hantz, D., Pedraza, O., Cornejo, R., Guinau, M., García-Sellés, D., Blanco, L., Gili, J. A., and Palau, J.: Rockfall Magnitude-Frequency Relationship Based on Multi-Source Data from Monitoring and Inventory, Remote Sensing, 15, 1981, https://doi.org/10.3390/rs15081981, 2023.

Khazaradze, G., Guinau, M., Blanch, X., Abellán, A., Tapia, M., Furdada, G., and Suriñach, E.: Multidisciplinary studies of the Puigcercos historical landslide in the Catalan Pyrenees, , https://doi.org/10.5194/egusphere-egu2020-7796, 2020.

Kogure, T., Aoki, H., Maekado, A., Hirose, T., and Matsukura, Y.: Effect of the development of notches and tension cracks on instability of limestone coastal cliffs in the Ryukyus, Japan, Geomorphology, 80, 236–244, https://doi.org/10.1016/j.geomorph.2006.02.012, 2006.

Loew, S., Hantz, D., and Gerber, W.: 5.09 - Rockfall Causes and Transport Mechanisms - A Review, in: Treatise on Geomorphology (Second Edition), edited by: Shroder, J. (Jack) F., Academic Press, Oxford, 137–168, https://doi.org/10.1016/B978-0-12-818234-5.00066-3, 2022.

Mainieri, R., Eckert, N., Corona, C., Lopez-Saez, J., Stoffel, M., and Bourrier, F.: Limited impacts of global warming on rockfall activity at low elevations: Insights from two calcareous cliffs from the French Prealps, Progress in Physical Geography: Earth and Environment, 47, 50–73, https://doi.org/10.1177/03091333221107624, 2023.

Melzner, S., Conedera, M., Hübl, J., and Rossi, M.: Lessons learnt from a rockfall time series analysis: data collection, statistical analysis, and applications, Nat. Hazards Earth Syst. Sci., 23, 3079–3093, https://doi.org/10.5194/nhess-23-3079-2023, 2023.

MEZAP: Caractérisation de l'aléa rocheux, BRGM, 68 pp., ISBN 978-2-7159-2760-5, 2021.

Mohadjer, S., Ehlers, T. A., Nettesheim, M., Ott, M. B., Glotzbach, C., and Drews, R.: Temporal variations in rockfall and rock-wall retreat rates in a deglaciated valley over the past 11 k.y., Geology, 48, 594–598, https://doi.org/10.1130/G47092.1, 2020.

Moos, C., Bontognali, Z., Dorren, L., Jaboyedoff, M., and Hantz, D.: Estimating rockfall and block volume scenarios based on a straightforward rockfall frequency model, Engineering Geology, 309, 106828, https://doi.org/10.1016/j.enggeo.2022.106828, 2022.

https://doi.org/10.5194/egusphere-2025-6247
Preprint. Discussion started: 22 December 2025

Phillips, C. and Walton, G.: Statistical analysis of factors influencing overall rockfall activity and the spatially-normalized rockfall power law activity constant, A, Engineering Geology, 357, 108297, https://doi.org/10.1016/j.enggeo.2025.108297, 2025.

Popescu, M. E.: A suggested method for reporting landslide causes, Bulletin of the International Association of Engineering Geology, 50, 71–74, https://doi.org/10.1007/BF02594958, 1994.

Pratt, C., Macciotta, R., and Hendry, M.: Quantitative relationship between weather seasonality and rock fall occurrences north of Hope, BC, Canada, Bull Eng Geol Environ, 78, 3239–3251, https://doi.org/10.1007/s10064-018-1358-7, 2019.

Priest, S. D. and Hudson, J. A.: Estimation of discontinuity spacing and trace length using scanline surveys, International Journal of Rock Mechanics and Mining Sciences & Geomechanics Abstracts, 18, 183–197, https://doi.org/10.1016/0148-9062(81)90973-6, 1981.

Rat, M.: Optimisation de la gestion de la route du littoral à la Réunion vis-à-vis du risque de chutes de blocs, BLPC, 43–52, https://hal.science/hal-05157014v1/file/aer000001757.pdf, 2006.

Royán, M. J., Abellán, A., and Vilaplana, J. M.: Progressive failure leading to the 3 December 2013 rockfall at Puigcercós scarp (Catalonia, Spain), Landslides, 12, 585–595, https://doi.org/10.1007/s10346-015-0573-6, 2015.

Ruiz-Carulla, R. and Corominas, J.: Analysis of Rockfalls by Means of a Fractal Fragmentation Model, Rock Mech Rock Eng, 53, 1433–1455, https://doi.org/10.1007/s00603-019-01987-2, 2020.

Santana, D., Corominas, J., Mavrouli, O., and Garcia-Sellés, D.: Magnitude–frequency relation for rockfall scars using a Terrestrial Laser Scanner, Engineering Geology, 145–146, 50–64, https://doi.org/10.1016/j.enggeo.2012.07.001, 2012.

Scavia, C., Barbero, M., Castelli, M., Marchelli, M., Peila, D., Torsello, G., and Vallero, G.: Evaluating Rockfall Risk: Some Critical Aspects, Geosciences, 10, https://doi.org/10.3390/geosciences10030098, 2020.

Schneider, M., Oestreicher, N., Ehrat, T., and Loew, S.: Rockfall monitoring with a Doppler radar on an active rockslide complex in Brienz/Brinzauls (Switzerland), Nat. Hazards Earth Syst. Sci., 23, 3337–3354, https://doi.org/10.5194/nhess-23-3337-2023, 2023.

Van Veen, M., Hutchinson, D. J., Kromer, R., Lato, M., and Edwards, T.: Effects of sampling interval on the frequency - magnitude relationship of rockfalls detected from terrestrial laser scanning using semi-automated methods, Landslides, 14, 1579–1592, https://doi.org/10.1007/s10346-017-0801-3, 2017.

Williams, J. G., Rosser, N. J., Hardy, R. J., and Brain, M. J.: The Importance of Monitoring Interval for Rockfall Magnitude-Frequency Estimation, Journal of Geophysical Research: Earth Surface, 124, 2841–2853, https://doi.org/10.1029/2019JF005225, 2019.

Wyllie, D. C.: Rock fall engineering, First issued in paperback., CRC Press Taylor & Francis Group, Boca Raton London New York, 243 pp., 2017.

Wyllie, D. C.: Rock slope engineering: civil applications, Fifth edition., CRC Press, Boca Raton, Florida, 2018.